Astron. Astrophys. 355, 1122–1128 (2000)

ASTRONOMY AND ASTROPHYSICS

Dust emission from star-forming regions

VI. The submillimetre YSO cluster in NGC 2264

D. Ward-Thompson[1], **R. Zylka**[2,3], **P.G. Mezger**[2], **and A.W. Sievers**[4]

[1] Department of Physics & Astronomy, University of Wales Cardiff, P.O. Box 913, Cardiff, UK
[2] Max-Planck-Institut für Radioastronomie, Auf dem Hügel 69, 53121 Bonn, Germany
[3] Institut für Theoretische Astrophysik, Tiergartenstrasse 15, 69121 Heidelberg, Germany
[4] IRAM, Avenida Divina Pastora 7, Nucleao Central, 18012 Granada, Spain

Received 13 August 1998 / Accepted 29 November 1999

Abstract. We present new submillimetre and millimetre continuum observations of NGC 2264, in the region of Allen's infra-red source IRS1, at 350, 450, 800 and 1300μm taken with the 15-m JCMT and the IRAM 30-m MRT. We observe a ridge of bright submillimetre and millimetre emission which we designate NGC 2264 MM. Within this ridge we have discovered a cluster of five submillimetre sources which we label NGC 2264 MMS1–5. The masses of the sources lie in the range $\sim$10–50M$_\odot$ and each source has a FWHM of $\leq$0.1pc. The total mass of the ridge is $\sim$730M$_\odot$.

We identify MMS3 as harbouring the driving source of a previously discovered bipolar outflow. We note that MMS5 is positionally coincident with a previously discovered HST near-ir source, but we conclude that this is a chance alignment, since typical extinction values within the ridge lie in the range A_V $\sim$200-1600. The cluster which we have discovered is of higher mass and extends over a larger area than the low-mass sub-cluster discovered by the HST surrounding IRS1. Our continuum maps show a greater dynamic range than molecular spectral line maps, due to gas freezing out onto dust grains at the densities of these sources. We suggest that each of the sources MMS1–5 is forming one or more intermediate or high mass stars.

Key words: stars: formation – ISM: dust, extinction – Galaxy: open clusters and associations: individual: NGC 2264

1. Introduction

NGC 2264 consists of an open cluster of O- and B-type stars at a distance of 800pc (Raimond 1966), and an extensive giant molecular cloud (eg: Krügel et al. 1987). Optical images show the famous cone nebula on the southern edge of the NGC 2264 molecular cloud. Roughly 3 arcmin to the north of the cone nebula there is an infrared source, designated IRS1, which was first discovered at 2 μm by Allen (1972). Inspection of the POSS red plate in the vicinity of IRS1 shows extensive nebulosity, but no optical counterpart, and the estimated extinction towards IRS1 is A_V $\sim$26 (Allen 1972). IRAS subsequently detected the point source IRAS06384+0932, which contains IRS1 within its error ellipse. A 2-μm survey of the whole NGC 2264 complex (Lada et al. 1993) identified around 360 near-ir sources believed to be forming an embedded cluster.

An ammonia survey of NGC 2264 revealed two main components of the cloud (Krügel et al. 1987), of which the southern component, NGC 2264-south, is roughly coincident with IRS1. NGC 2264-south is qualitatively similar to, but somewhat more massive than typical ammonia cores observed elsewhere (eg: Benson & Myers 1989, and references therein). High-velocity gas, red-shifted to velocities of $\sim$10–15 kms^{-1}, was detected in CO (Margulis et al. 1988), with a peak in the red-shifted emission some 30 arcsec to the south of IRS1, and designated NGC 2264 C. However, it was not clear that this was a bipolar outflow, as only the red lobe was observed.

More recently, Schreyer et al. (1997) carried out a detailed molecular line study of this region and identified two bipolar outflows, one associated with IRS1, and one associated with a deeply embedded cluster they observed in this region in the near-infrared K-band. This region was subsequently observed with the HST NICMOS camera by Thompson et al. (1998), who identified six new sources in this cluster as pre-main-sequence stars.

In this series of papers, we have reported on an observing program of millimetre continuum emission from star forming regions. The scientific objectives include ascertaining the physical parameters of these regions and hence gaining a deeper insight into the star formation process. In this paper we attempt to ascertain the evolutionary status of the objects in the NGC 2264 region. We have obtained 1.3-mm continuum data with the IRAM 30-m MRT, and 800-, 450- & 350-μm continuum data with the JCMT.

2. Observations and data reduction

Observations at 1.3mm were performed in February 1992, using the IRAM 30-m telescope (MRT) on Pico Veleta, Spain and the 7-channel bolometer array (Kreysa 1994). The seven beams of the bolometer array are arranged in a hexagon around the central beam with spacings of $\sim 20''$. Chopping was provided by

Table 1. Mapping parameters of the data of NGC 2264 taken with both the MRT and the JCMT at 1300, 800, 450 & 350 μm.

Wavelength (μm)	No. of maps	Int. time /pixel (s)	Beam FWHM (arcsec)	Pixel size (arcsec)	Chop throw (arcsec)	Map extents (arcmin)	Final rms (Jy/beam)
1300	1	1	12	4	30	4×3	0.02
800	4	1	13	4	40	3.5–5×4.5–3	0.2
450	5	1	8	3	20	2.7–4.6×3.6–2	1.5
350	3	1	6	3	20	2.5×3.5–4	2.0

wobbling the secondary mirror in azimuth at 2 Hz with a throw of 30″. The 225GHz atmospheric opacity was monitored using 'skydips' and was found to be 0.18 during the observations. The map parameters are listed in Table 1.

Observations at 800, 450 and 350 μm were carried out at the James Clerk Maxwell Telescope[1] (JCMT), located on Mauna Kea, Hawaii, during the evening shifts of 1993 February 25 to 28, 17:30–01:30 HST (UT = 03:30–11:30). The detector used was the common-user receiver UKT14, which contains a single-element, ^{3}He-cooled Ge:In:Sb bolometer, and a series of filters matched to the atmospheric transmission windows (Duncan et al. 1990). The observations were carried out while using the secondary mirror to chop in azimuth at around 7 Hz and synchronously to detect the signal, thus rejecting 'sky' emission. Photometry was carried out using a chop throw of 60 arcsec and a FWHM beam-size of 18 arcsec throughout. Maps were made in dual-beam 'on-the-fly' raster mode, where the telescope is scanned in azimuth and elevation, while simultaneously chopping in azimuth, using chop throws of 40, 20 and 20 arcsec and diffraction-limited FWHM beam-sizes of 13, 8 and 6 arcsec at 800, 450 and 350 μm respectively. The map parameters are listed in Table 1. Note that all maps used a sampling rate step size less than half of the FWHM beam-size, to ensure that all maps were over-sampled.

Calibration was performed using the planet Mars, whose assumed brightness temperatures were taken from Griffin et al. (1986), Orton et al. (1986) and Griffin & Orton (1993), and which was observed in all wavebands at least once per hour, to measure the detector sensitivity at each waveband. In addition, beam maps were made of the planet at each waveband using exactly the same mapping parameters as for the maps of NGC 2264, to calibrate the maps of NGC 2264, and to estimate the effect of the error-beam of the telescope at the shorter wavelengths on extended source flux measurements. Throughout the observations, estimates were obtained of the atmospheric opacity at each waveband, based on the monitoring of the opacity at 225 GHz provided by the NRAO radiometer, located at the Caltech Submillimetre Observatory (CSO), using standard formulae (Sandell 1994; Stevens & Robson 1994).

The 225 GHz atmospheric opacity at zenith was fairly stable at around 0.025–0.05 throughout our observations, which is typical of good conditions at the site. This continuous monitoring of a calibration source of known intensity, together with the 225 GHz opacity, allowed the atmospheric opacity, τ, to be calculated at all times in all wavebands, and a fully consistent calibration was obtained. Altogether, we estimate our total absolute calibration uncertainty to be $\sim$ 20 per cent at 1300 & 800 μm, $\sim$30 per cent at 450 and $\sim$40 per cent at 350 μm. Pointing and focus checks were performed typically once per hour. The focus was found to be very stable throughout, and the pointing was observed to be accurate to better than 3 arcsec.

The raw double-beam maps were created using the tasks MAKMAP and MAKE_MAP for the MRT and JCMT data respectively. The subsequent data reduction was performed using the software package MAP (Zylka 1995). First the double-beam maps were automatically despiked and a base-plane was subtracted. This base-plane was defined using identical emission-free areas around the edges of the maps. Before restoring to single-beam maps, using an improved version of the algorithm of Emerson, Klein and Haslam (1979), the extinction corrections were performed and the emission-free areas were masked (i.e. not used during the following data reduction). This masking reduced the noise in the restored maps by up to 10%, depending on the size ratio of the unmasked to masked areas. The individual maps at each particular frequency were averaged while transforming from the horizontal to equatorial system. During this step the combined effects of pointing errors and errors due to anomalous refraction (Altenhoff 1987, Zylka et al. 1992, 1995) were corrected by shifting the maps in (Az,El). The shifts varied from 0.5″ to 2″. The single maps entered the average with weights proportional to $(\mathrm{rms})^{-2}$. The rms noise was calculated in the emission-free areas before masking, and the 1 σ level in the final maps was found to be 0.02, 0.2, 1.5 & 2 Jy per main beam (see Table 1) at 1300, 800, 450 & 350 μm respectively. After smoothing to 13 arcsec the 1 σ noise levels at 450 & 350 μm were found to be 1.5 & 2.6 Jy per 13-arcsec beam respectively.

3. Results

3.1. Maps

Fig. 1a–d shows isophotal contour maps, superposed on grey-scale images, of the NGC 2264 region at 1300, 800, 450 and 350 μm, all smoothed to 13-arcsec resolution, which is the lowest resolution of the raw data-sets – the 800-μm data. The origin of the maps is at (RA,Dec.) (1950) = (06^{h} 38^{m} 27.5^{s}, +09° 32′ 00″). The submillimetre continuum emission traces the cold

[1] The James Clerk Maxwell Telescope is operated by the Joint Astronomy Center, on behalf of the UK PPARC, the Netherlands Organisation for Pure Research, and the National Research Council of Canada.

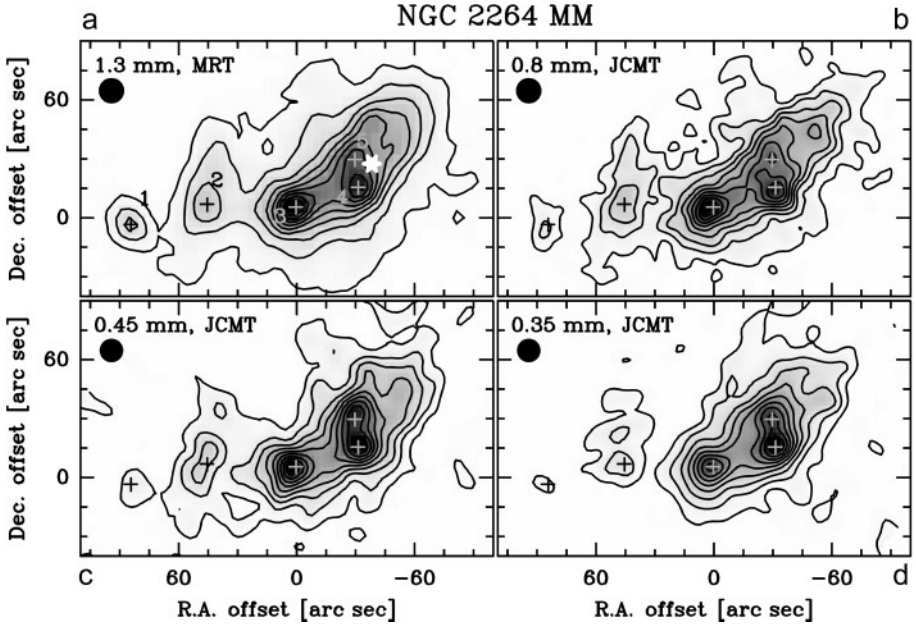

Fig. 1a – d. Isophotal contour maps superposed on grey-scale images of the 1300-, 800-, 450- & 350-μm continuum emission respectively, from NGC 2264 MM at 13 arcsec resolution. The (0,0) position is at RA (1950) = $6^h\ 38^m\ 27.5^s$, Dec (1950) = $+09^\circ\ 32'\ 00''$. The sources MMS 1–5 are labelled and the position of IRS1 is marked with a star in **a**. The circle on each plot represents the resolution to which the data have been smoothed. The contour levels in each case are plotted from 9% of the peak value to 99% of peak, in intervals of 10%.

dust in the molecular cloud and should delineate the extent of the cold cloud core. It can be seen that the morphology of the four maps looks very similar, and a number of features can be seen in the maps: A curved ridge of emission is seen extending for over 2 arcmin from north-west to south-east, and turning to the east. We here designate this ridge NGC 2264 MM. Within this ridge a number of compact sources are seen, in addition to other, more extended features. We here designate the compact sources NGC 2264 MMS1–5, and label them as such in Fig. 1a. In addition, we mark the position of the source IRS1 on Fig. 1a with a star.

The five sources appear somewhat different at each of the different wavelengths. MMS1 is clearly detected at 1300 μm, but is less obvious at the shorter wavelengths, due to their slightly lower signal-to-noise ratio. MMS2 appears elongated north-south at 1300 and 800 μm, but appears to break up at the shorter wavelengths. This may also be a result of the lower signal-to-noise ratio at 350 and 450 μm, and may be caused by anomalous refraction effects (see discussion in Appendix of Zylka et al 1995). MMS3 is seen clearly at all 4 wavelengths, with the same morphology. MMS4 & 5 appear to be only marginally resolved from one another at 13 arcsec resolution.

Fig. 2a and b shows isophotal contour maps, superposed on grey-scale images, of the central region of NGC 2264 MM at 450 and 350 μm, at 8 arcsec resolution, which is the full resolution of the JCMT at 450 μm. The 350-μm data have been smoothed to the same resolution for direct comparison. The three sources MMS3, 4 & 5 can all be clearly seen, and now MMS4 and MMS5 are resolved from one another.

3.2. Source parameters

Table 2 lists the flux densities of the five sources at each of the four wavelengths. Column 1 lists the source name and its position in absolute terms as well as its offset in arcsec from the (0,0) position of Fig. 1, and Column 2 lists the wavelength in microns. Column 3 lists the peak flux density in Jy/13-arcsec

Table 2. Flux densities in Jy of NGC 2264 MM, measured from the 13-arcsec resolution maps of Fig. 1. The positions of the sources are given both in absolute terms and as offsets from the (0,0) positions of the maps. The 1 σ noise levels are 0.02, 0.2, 1.5 & 2 Jy and the absolute calibration uncertainties are estimated to be 20, 20, 30 & 40% at 1300, 800, 450 & 350 μm respectively.

Source (Posn.)	λ (μm)	Peak flux (13” beam)	Flux in 20” diam. aper.
MMS1	1300	0.5	0.6
(+84.3”,−3.4”)	800	1.0	1.0
($06^h\ 38^m\ 33.0^s$	450	6.7	7.6
$+09^\circ\ 31'\ 56.6''$)	350	7.7	8.6
MMS2	1300	0.5	0.8
(+45.5”,+6.9”)	800	1.8	2.3
($06^h\ 38^m\ 24.5^s$	450	13.0	16.7
$+09^\circ\ 32'\ 06.9''$)	350	16.2	20.1
MMS3	1300	1.5	2.0
(+0.3”,+5.5”)	800	4.7	5.6
($06^h\ 38^m\ 27.5^s$	450	36.6	44.3
$+09^\circ\ 32'\ 05.5''$)	350	57.3	72.9
MMS4	1300	1.3	1.9
(−31.3”,+15.5”)	800	4.2	5.4
($06^h\ 38^m\ 25.4^s$	450	37.7	48.8
$+09^\circ\ 32'\ 15.5''$)	350	69.3	88.3
MMS5	1300	1.1	1.8
(−29.6”,+29.7”)	800	3.3	4.8
($06^h\ 38^m\ 25.6^s$	450	33.6	47.6
$+09^\circ\ 32'\ 29.7''$)	350	41.7	79.6

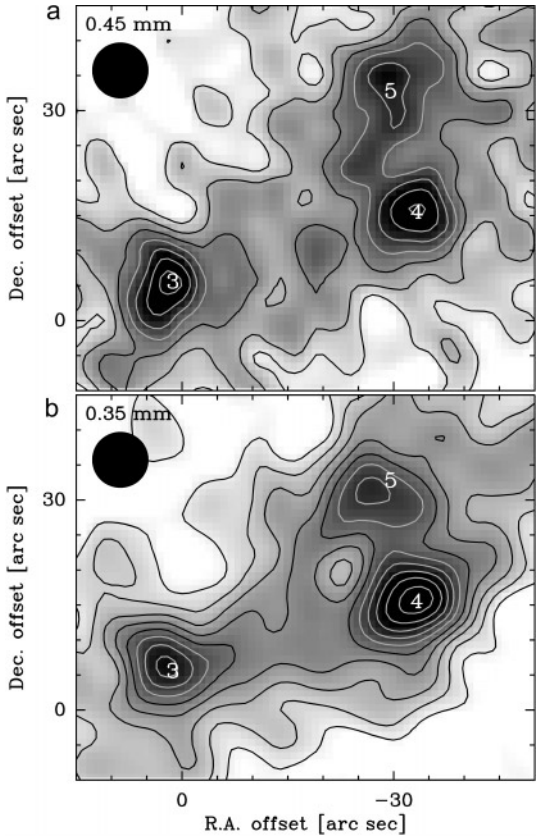

Fig. 2a and b. Isophotal contour maps superposed on grey-scale images of the submillimetre continuum emission from the central region of NGC 2264 MM at 450 and 350 μm respectively. These maps are now shown at 8-arcsec resolution (indicated by the circle on each plot), which is the diffraction limit at 450 μm, but means that the 350 μm data have been smoothed slightly. The (0,0) position is again at RA (1950) = $6^{\rm h}$ $38^{\rm m}$ $27.5^{\rm s}$, Dec (1950) = +09° 32′ 00″. In each case the base contour level is 3 Jy per 8-arcsec beam, and the contour interval is 3 Jy/beam.

beam measured on the peak of each source in Fig. 1. Column 4 lists the flux density in Jy measured in a 20-arcsec diameter aperture. Table 3 lists the total flux density measured in each map for the whole NGC 2264 MM ridge, together with the IRAS PSC flux densities (see also Margulis et al. 1989), and other data from Harvey et al. (1977).

It is seen clearly from Fig. 1 that each compact source sits on top of more extended emission. Thus, in an attempt to separate the compact sources from the more extended emission, we fitted the data with a number of two-dimensional gaussian components – one on each of the emission peaks. Table 4 lists the details of these gaussian fits. Column 1 gives the source name, while Columns 2 & 3 list the FWHM in arcsec and the position angle of the gaussian fit for each source. These were measured from the 13-arcsec resolution data of Fig. 1, and an average was taken. MMS1 & 2 were not detected at sufficiently high signal-to-noise ratio at 350 and 450 μm to measure their FWHM accurately, although they are clearly significantly extended, hence their FWHM were only measured on the 1300- and 800-μm data.

Table 3. Total flux densities for NGC 2264 MM in Jy measured from Fig. 1, together with total IRAS flux densities at 100 & 60 μm, as well as 175, 100 and 53 μm integrated flux densities from Harvey, Campbell & Hoffmann (1977).

λ (μm)	Total flux density
1300	26.7
800	97
450	421
350	835
100	1291
60	784
175	1530
100	1645
53	980

We note that the gaussian fits are not necessarily unique but they provide at least a physical size scale to associate with each source. Column 4 of Table 4 gives the deconvolved FWHM of the gaussian fits to each source in parsec. The sources themselves may not have a gaussian radial density profile, but this was felt to be the simplest way to separate compact emission from more extended emission. Column 5 lists the flux density at 800 μm within the FWHM of the gaussian fits to give a feel for how the flux densities of Table 2 scale. The gaussian decomposition was performed using the AIPS task IMFIT, and cross-checked with the STARLINK task GAUFIT, which gave consistent results.

3.3. Spectral energy distribution

Fig. 3 shows a plot of F_ν versus ν, on a logarithmic scale, for the whole of NGC 2264 MM using the flux densities listed in Table 3, in the infrared and submillimetre regimes. The thick solid line fitting the data for the whole cloud is the sum of two modified black-body curves, each of the form:

$$S(\nu) \; = \; \Omega_\nu B(\nu, T)(1 - e^{-\tau}) \qquad (1)$$

where Ω_ν is the effective solid angle of the source, B(ν, T) is the Planck function and $\tau = (\nu/\nu_c)^\beta$ is the optical depth. ν_c is the critical frequency at which the optical depth equals 1, with corresponding wavelength λ_o, and β is the dust grain opacity (Hildebrand 1983). It was not possible to fit all of the submillimetre and far-infrared data of the whole NGC 2264 MM region with a single temperature grey-body curve, two being the minimum required to fit the data. The warmer grey-body has a temperature of 38 K, and is consistent with the FIR data. The cooler grey-body has a temperature of 17 K and is consistent with the mm/submm data. Consequently, when deriving dust and gas masses from the submillimetre continuum data, we will use a dust temperature of 17 K since it is always the coldest dust component which dominates the mass.

Table 4. Source parameters: The FWHM sizes of the sources were estimated by fitting gaussians to the data in Fig. 1, and deconvolved in quadrature with a 13-arcsec beam-size. The FWHM were converted to pc assuming a distance of 800 pc. The flux densities in Jy within the FWHM are quoted at 800 μm to show how these vary relative to the values listed in Table 2. The masses are calculated as described in the text, quoted to 2 significant figures, and the column and volume densities listed are the mean densities within the FWHM.

Source Name	FWHM (arcsec)	PA ±5 ($^\circ$)	Deconvolved FWHM (pc)	Flux density	Mass ($M_\odot$)	N(H_2) $\times 10^{23}$ cm^{-2}	n(H_2) $\times 10^6$ cm^{-3}
MMS1	20×16	10	0.06×0.04	1.0	7.5	2.5	2.5
MMS2	31×24	167	0.11×0.08	2.5	19	1.6	0.8
MMS3	28×18	116	0.10×0.05	6.4	48	7.3	4.8
MMS4	20×17	31	0.06×0.04	6.2	47	15.8	15.7
MMS5	23×15	132	0.08×0.03	5.7	43	14.7	14.5

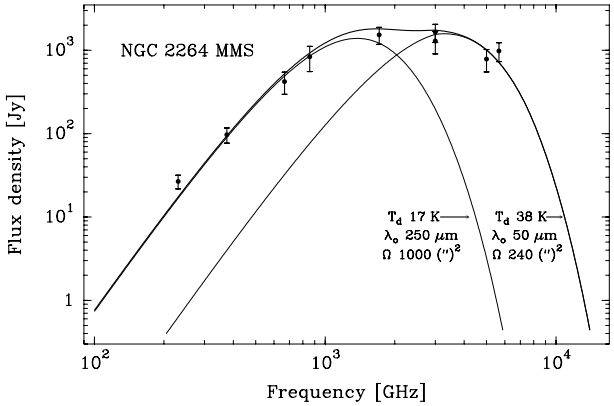

Fig. 3. Plot of F_ν/Jy versus ν/GHz, on a logarithmic scale, for the whole of NGC 2264 MM, using the data in Table 3.

We can speculate as to the nature of the warm dust component. We see from the fit that it has a smaller solid angle than the cold dust component, and hence is more compact. It is also, of course, hotter. Therefore we hypothesise that this dust originates in one or more discrete regions close to some central heating sources in the cloud. We discuss below the evidence that star formation has already begun in this cloud, and we merely note here that the existence of the warm dust component corroborates this picture. We also note that the longest wavelength data-point in Fig. 3 lies slightly above the best fit curve to the remainder of the data. This may be tentative evidence for the presence of a free-free component of the emission at long wavelengths, which could also be pointing to already forming stars. However, observations at radio wavelengths would be required to confirm this.

4. Discussion

4.1. Physical parameters

To derive masses from the optically thin dust continuum flux densities listed in Table 4, we use the formulation of Hildebrand (1983), modified to a form involving the mass opacity κ, such that:

$$M_g = \frac{F(\nu)D^2}{\nu^3\kappa(2h/c^2)}[\exp(h\nu/kT) - 1]$$

where M_g is the total gas mas, D is the source distance (800 pc), and the mass opacity κ is normalised such that its value at 800μm is 0.009 cm^2/g. All other parameters take their usual meanings. A mean mass for each source was calculated from the gaussian flux densities at all wavelengths, assuming the dust temperature derived above of 17 K, and is listed in Table 4. The column and volume densities were then derived, averaged over the FWHM of each source, and these too are given in Table 4.

4.2. Comparison with previous studies

We can compare our maps in Figs. 1 & 2 with data at other wavelengths. Sargent et al. (1984) showed 70- & 130-μm images of NGC 2264 taken with 3-arcmin resolution, and saw simply a single source. Schwartz et al. (1985) showed a 170-μm image of NGC 2264 taken with a 68-arcsec beam, and also saw only a single source, but with a slight E-W elongation. Both datasets are consistent with our data smoothed to much lower resolution. However, our data appear inconsistent with the partial map made at 1.3 mm by Schwartz et al. (1989). Also the $C^{18}O$ data of the region of Schwartz et al. (1989) appear to show only approximate morphological agreement, with a single, marginally elongated source, but with the elongation at a different position angle from NGC 2264 MM. Likewise the ^{12}CO and ^{13}CO data of Sargent et al. (1984) show no apparent similarity to the submillimetre continuum data. The molecular line data of the region in the high density tracer NH_3 taken with 40-arcsec resolution by Krügel et al. (1987) show reasonable agreement with our data. An elongated source is seen, which is roughly coincident with NGC 2264 MM, although only one source is seen in the NH_3 data. In addition, the dynamic range observed in the NH_3 map is considerably less than is seen in our millimetre and submillimetre continuum maps.

The more recent higher resolution CO and CS isotope data of Schreyer et al. (1997) show somewhat similar morphologies, with different sources being apparent in different tracers, and no one tracer showing all of the sources visible in the continuum. Likewise, their data do not extend as far as MMS1 & 2. However, MMS3 can be seen in their IRAM $C^{18}O$ (2−1) data as well as in their JCMT CS (7−6) and CH_3OH data.

The dynamic range of the NH_3, CS and CO maps is less than that seen in the submillimetre continuum. This is similar to

the finding for NGC 2024 (Mauersberger et al. 1992 – Paper III) that the embedded sources are seen much more clearly in the millimetre continuum than in $C^{34}S$ data. In that case the lower dynamic range in the $C^{34}S$ data was ascribed to gas freezing out onto dust grains in the high density core regions. A similar effect is probably occurring in NGC 2264 MM.

A comparison with the HST image of Thompson et al. (1998) shows that our source NGC 2264 MMS5 is almost exactly coincident with source number 4 of Thompson et al. (1998). However, their sources 5 and 6 also lie within the FWHM of MMS5. If one of these three sources is in reality our source MMS5, then clearly its near-ir extinction has been considerably under-estimated by Thompson et al. (1998). It is more likely that all three sources are simply foreground to the dense dust condensation of MMS5, and that the positional association is pure chance, since with the column densities and A_V values we calculated above, the near-infrared sources cannot be background. There is nothing visible in the HST image at the position of MMS4, and the other three submillimetre sources are outside of the bounds of the published HST image.

4.3. The nature of the sources

Clearly these are high mass condensations with high column densities, which correspond to visual extinctions (under the usual typical assumptions) of $A_V \sim 200-1600$ mag. These individual 'sources' which we have labelled may well each form multiple stars. However, the mean densities are typical of dense cores in molecular clouds. The total mass associated with the total flux densities listed in Table 3 corresponds to about 730 $M_\odot$ for the whole ridge.

A comparison can be made of the CS (5−4) data taken at JCMT by Schreyer et al. (1997) with our submillimetre continuum data. Their Fig. 6 shows two outflows are detected in CS (5−4), one centred on IRS1, and the other offset to the south-east, and observed by Schreyer et al. (1997) to be offset slightly from a K-band source they observe. We can see by comparison with our data that this second outflow is centred on MMS3, and we here postulate that NGC 2264 MMS3 is the driving source of this second outflow in the region. Hence we postulate that MMS3 has already formed a young stellar object (YSO) at its centre and may be a high mass equivalent of a Class 0 protostar.

The masses of MMS3, 4 & 5 are all $\sim$40–50$M_\odot$, and so all may be forming multiple stars of intermediate to high mass. MMS1 & 2 are of slightly lower mass, and are somewhat detached from the main ridge in which the other sources are embedded. However, these two still contain sufficient mass to form multiple stars of intermediate mass, or one high-mass star each. None of these objects has a detected bipolar outflow yet. We therefore hypothesise that each of these is pre-protostellar in nature, and that a very rich cluster of intermediate and high mass stars is in the process of forming in the NGC 2264 MM region.

The infrared source IRS1 is believed to be a 9.5$M_\odot$ B2 zero-age main-sequence (ZAMS) star (Allen 1972), with a visual extinction of $\sim$20–30 (Thompson et al. 1998). Since we have derived extinction values $>$200 towards our five MMS sources, we conclude that IRS1 must have formed on the near-side of this cluster. However, the positional association of IRS1 with the MMS sources is clearly not coincidental, and they are part of the same cluster. Furthermore the mass estimate of IRS1 of $\sim$10$M_\odot$ is comparable to the masses of the stars which we postulate are forming in the NGC 2264 MM cluster. The fact that IRS1 (Margulis et al. 1988) and MMS3 (Schreyer et al. 1997) both power bipolar outflows also argues that these sources are at a similar evolutionary state. However, the outflow from MMS3 is smaller in spatial extent, and is less luminous, which leads us to postulate that MMS3 may be slightly less evolved than IRS1. The remaining sources may also have outflows, but may be more embedded, and hence as yet undetected. Alternatively, they may be at a still earlier evolutionary state. The source IRS1 has been postulated to have triggered the formation of a small, low-mass cluster of stars (Thompson et al. 1998) foreground to our (sub)millimetre sources, but we can now address the question of what formed the (sub)millimetre cluster we have observed.

NGC 2264 is a part of the Mon OB1 Stellar Loop, which includes NGC 2261 and NGC 2259, and which is hypothesised to be a shell of swept-up material surrounding a SNR or OB association (Schwartz 1987). Within this shell of shock-compressed material, triggered high-mass star formation then occurs. Close comparison of our Fig. 1 with Fig. 1 of Schwartz (1987) shows that the extended ridge which we see in the millimetre and submillimetre is well aligned with the large-scale IRAS 100-μm emission which traces the Mon OB1 Stellar Loop around most of its circumference. We therefore here hypothesise that the ridge which we have observed is part of this loop and is caused by the same SNR or OB association wind, and the associated shock compression has triggered star formation in this region, causing the formation of IRS1, MMS 1–5 and a number of lower mass stars.

5. Summary

We have mapped the region around NGC2264-IRS1 at 350, 450, 800 & 1300 μm. We have observed a region of bright submillimetre and millimetre emission which we have designated NGC 2264 MM. Within this region we have discovered a cluster of five submillimetre sources which we have labelled NGC 2264 MMS1–5. These sources represent previously unkown condensations of dust and gas, whose masses range from $\sim$10–50$M_\odot$, with visual extinctions of $\sim$200–1600 magnitudes. Consequently they have no optical counterparts, and do not correlate well with near-ir data or with molecular spectral line data. We hypothesise that each source is in the process of forming one or more intermediate or high mass stars.

Acknowledgements. The authors wish to thank the staff of the Joint Astronomy Centre, Hawaii, for their assistance while JCMT observations were carried out. The British Council and the DAAD are gratefully acknowledged for travel funding, under the ARC programme, during the data reduction phase and writing of this manuscript.

References

Allen D.A., 1972, ApJ 172, L55

Altenhoff W.J., Baars J.W.M., Downes D., Wink J.-E., 1987, A&A 184, 381

Benson P.J., Myers P.C., 1989, ApJ Suppl. 71, 89

Duncan W.D., Robson E.I., Ade P.A.R., Griffin M.J., Sandell G., 1990, MNRAS 243, 126

Emerson D.T., Klein U., Haslam C.G.T., 1979, A&A 76, 92

Griffin M., Orton G.S., 1993, Icarus 105, 537

Griffin M.J., Ade P.A.R., Orton G.S., et al., 1986, Icarus 65, 244

Harvey P.M., Campbell M.F., Hoffmann W.F., 1977, ApJ 215, 151

Hildebrand R.H., 1983, QJRAS 24, 267

Krügel E., Güsten R., Schulz A., Thum C., 1987, A&A 185, 283

Kreysa E., 1994, in: Guyenne T.D. (ed.), Photon Detectors for Space Instrumentation, ESA/ESTEC, Noordwijk

Lada C.J., Young E.T., Greene T.P., 1993, ApJ 408, 471

Margulis M., Lada C.J., Snell R.L., 1988, ApJ 333, 316

Margulis M., Lada C.J., Young E.T., 1989, ApJ 345, 906

Orton G.S., Griffin M.J., Ade P.A.R., et al., 1986, Icarus 67, 289

Raimond E., 1966, Bulletin of the Astronomical Institute of the Netherlands 18, 191

Sandell G., 1994, MNRAS 271, 75

Sargent A.I., van Duinen R.J., Nordh H.L., Fridlund C.V.M., Aalders J.W., Beintema D., 1984, A&A 135, 377

Schreyer K., Helmich F.P., van Dishoek E.F., Henning Th., 1997, A&A 326, 347

Schwartz P.R., Thronson H.A., Odenwald S.F., Glaccum W., Loewenstein R.F., Wolf G., 1985, ApJ 292, 231

Schwartz P.R., Snell R.L., Schloerp F.P., 1989, ApJ 336, 519

Schwartz P.R., 1987, ApJ 320, 258

Stevens J.A., Robson E.I., 1994, MNRAS 270, L75

Thompson R.I., Corbin M.R., Young E., Schneider G., 1998, ApJ 492, L177

Zylka R., Mezger P.G., Lesch H., 1992, A&A 261, 119

Zylka R., Mezger P.G., Ward-Thompson D., Duschl W.J., Lesch H., 1995, A&A 297, 83

Zylka R., 1995, Pocket Cookbook for Mapping Software. MPIfR Report